J Mol Model (2015) 21: 207
DOI 10.1007/s00894-015-2749-3

ORIGINAL PAPER

Hydrogen abstraction mechanisms and reaction rates of toluene+NO_3

Yongmei Ma[1,2] · **Kehe Su**[1] · **Jin Zhang**[1] · **Yanli Wang**[1] · **Xin Wang**[1] · **Yan Liu**[1,2]

Received: 29 March 2015 / Accepted: 29 June 2015 / Published online: 23 July 2015

Abstract The hydrogen abstraction reaction mechanisms of toluene molecule by NO_3 radical were investigated theoretically with quantum chemistry and reaction kinetics. All the molecular structures, vibrational properties, and the intrinsic reaction coordinates were determined with B3LYP/6-311G(d,p). The non-dynamic electronic correlations were examined with the CASSCF dominant configurations. The energies and the potential energy profiles were refined with accurate model chemistry G3(MP2). Rate constants were determined using the CVT method over the temperature range 200–2000 K. It was found that in addition to the side chain H-abstraction, the ring H-abstraction reactions are also possible. The side chain H-abstraction rate constant is in very good agreement with the available experiments and has a non-Arrhenius characteristic. Nevertheless, all the ring H-abstractions follow the Arrhenius behavior well. The over-all reaction was found to have a complex reaction mechanism in which the side chain H-abstraction is dominant below 700 K while the ring H-abstractions are competitive above 800 K. The approximate apparent activation energies E_{app} are 15.5 and 66.4 kJ mol^{-1} at 300–700 K and 800–2000 K, respectively.

✉ Kehe Su
sukehe@nwpu.edu.cn

[1] Key Laboratory of Space Applied Physics and Chemistry of the Ministry of Education, School of Natural and Applied Sciences, Northwestern Polytechnical University, Xi'an, Shaanxi 710072, People's Republic of China

[2] College of Chemistry and Life Sciences, Weinan Normal University, Weinan, Shaanxi 714009, People's Republic of China

Keywords Canonical variational transition-state theory · Hydrogen abstraction · Rate constant · Reaction rate · Tunneling effect

Introduction

Volatile organic compounds (VOCs) have been a major concern due to their chemical compositions within the atmosphere in the lower atmosphere and troposphere where aromatic hydrocarbons always contribute a significant fraction (about 20 %) of the total VOCs in the polluted atmosphere in the urban areas [1]. The main emission sources of the aromatics are motor vehicle exhaust, evaporation of solvents, and the emission in the gasoline stations [2–4]. In addition to the important role in the photochemical production of ozone, oxidation of aromatic compounds leads to the formation of secondary organic aerosol (SOA) in the urban air [5], which is well known to be harmful to human health [6].

Toluene is one of the most abundant aromatic hydrocarbons in the urban atmosphere [7]. Its most important loss process is initiated by OH radical during daylight hours and by nitrogen trioxide NO_3 radical during evening and nighttime hours [8–10]. The reactions of toluene with OH have been studied widely both experimentally [11–17] and theoretically [18, 19]. The NO_3-initiated toluene oxidation reactions have also been investigated in the experiments of Carter and co-workers [20] and Atkinson and co-workers [21–24]. The upper limit of the rate constant of $NO_3+C_6H_5CH_3$ was reported as $\leqq 3\times10^{-15}$-8×10^{-15} $cm^3\cdot molecule^{-1}\cdot s^{-1}$ determined at 300±1 K in 1981 [20]. A smaller value of $(1.8\pm1.0)\times10^{-17}$ $cm^3\cdot molecule^{-1}\cdot s^{-1}$ at 296±2 K determined by using a relative rate technique was also reported, and suggested for the methyl H-abstraction constant in 1984 [21]. Shortly

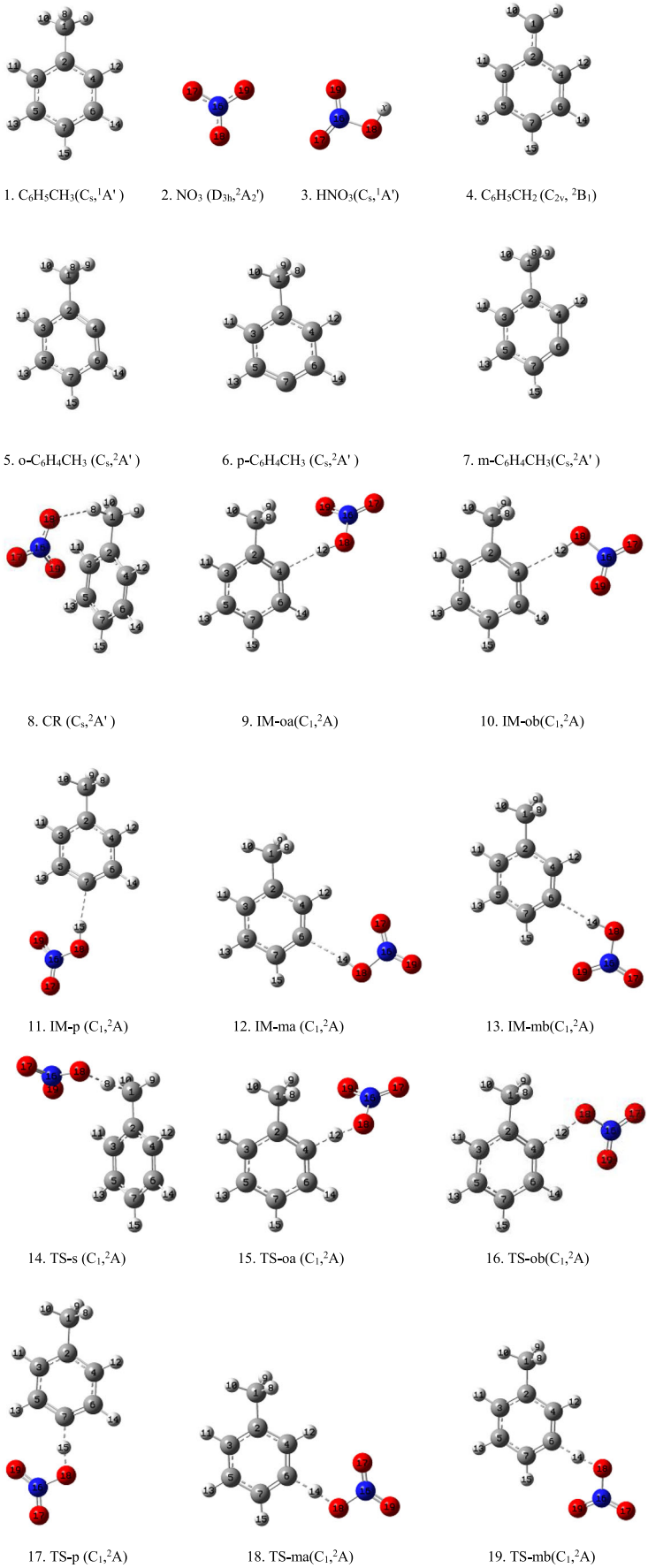

Fig. 1 Structure, symmetry and the electronic state of the reactants, products, intermediates and transition states for the reaction of toluene with NO_3 obtained with B3LYP/6-311G(d,p) calculations

in the same year, it was refined to be $(2.0\pm1.1)\times10^{-17}$ $cm^3 \cdot molecule^{-1} \cdot s^{-1}$ at 298±1 K with two different techniques by monitoring the enhanced decay rates of N_2O_5 and by employing a relative rate in the reaction system [22]. For the temperature at 296±2 K, a slightly larger rate constant $(7.8\pm1.5)\times10^{-17}$ $cm^3 \cdot molecule^{-1} \cdot s^{-1}$ was reported in 1988 [23]. Recently in 2007, the reaction of NO_3 radical with deuterium substituted toluene-d3 ($C_6H_5CD_3$) and toluene-d8 ($C_6D_5CD_3$) implied [24] that both hydrogen abstraction from the substituent group and the ortho addition may proceed at room temperature. It was also found that the ortho addition may decompose back to the reactants [24] but the rate constants have not been developed.

In the point of view of chemical reactions, the hydrogen atom can be abstracted either from the -CH_3 group or from the benzene ring, and four different NO_3-toluene adduct isomeric radicals can be formed. The H-abstraction abstractions will lead to the formation of benzyl and methylphenyl radicals which can associate with O_2 and produce benzylperoxy and methylphenylperoxy radicals in the presence of molecular oxygen. These association processes are exothermic and the reaction enthalpies are 91.4±4 kJ mol^{-1} [25] and 196.1 kJ mol^{-1} [26], respectively. Ref. [26] also reported that the methylphenyl radical can isomerize into the more stable benzyl radical via intramolecular hydrogen shift reaction at higher temperatures. Although the reaction paths and rate constants of benzyl and methylphenyl radicals with O_2 have been explored [26, 27] the detailed information of the formation of benzyl and methylphenyl radicals in the reaction system of NO_3-toluene has not been obtained so far.

This work is, thus, aimed at carrying out a theoretical investigation on all of the possible initial steps of NO_3-toluene hydrogen abstraction reactions, in which some of the results can be compared with the available experiments, develop the temperature dependent rate constants, and explore the over-all reaction rate. In order to emphasize the details of the H-abstractions, the addition reactions of toluene and NO_3 radical will be reported in a separate work.It should be noted that just after this paper had been accepted for publication we noted Huang and coworkers [28] published a theoretical study of a similar reaction system with CCSD(T)/6-311++G(d,p)//BHandHLYP/6-311++G(d,p) method. The main results will also be compared.

Computational methods

All the geometries of the stable species and the transition states (TSs) were fully optimized with the B3LYP [29, 30] density functional theory combined with the 6-311G(d,p)

Table 1 G3(MP2) energy (sum of electronic energy and ZPE, in atomic unit: a.u.), the enthalpy correction ($H_{corr.}$, without ZPE) (a.u.), the Gibbs free energy correction ($G_{corr.}$, without ZPE) (a.u.) at 298.15 K and their relative (with respect to the sum of the reactants) values (in kJ mol^{-1}) calculated with the standard statistical thermodynamics

Number	Species	E (G3MP2) a.u.	$\Delta U_{0\ K}$ kJ mol^{-1}	$H_{corr.}$	ΔH_{298} kJ mol^{-1}	$G_{corr.}$	ΔG_{298} kJ mol^{-1}
1	$C_6H_5CH_3$	−271.068022		0.007350		−0.031016	
2	NO_3	−279.922067		0.004913		−0.025033	
3	HNO_3	−280.585544		0.004526		−0.025785	
4	$C_6H_5CH_2$	−270.421050	−43.3[a]	0.006811	−45.8[a]	−0.029139	−40.4[a]
5	o-$C_6H_4CH_3$	−270.385666	49.6[a]	0.007333	48.5[a]	−0.030873	48.0[a]
6	p-$C_6H_4CH_3$	−270.384901	51.6[a]	0.007334	50.5[a]	−0.031055	49.5[a]
7	m-$C_6H_4CH_3$	−270.385686	49.5[a]	0.007335	48.5[a]	−0.031075	47.4[a]
8	CR[b]	−550.983996	−2.4	0.012601	−1.6	−0.041736	35.1
9	IM-oa	−550.979875	26.8	0.012863	28.4	−0.044055	58.3
10	IM-ob	−550.979625	27.5	0.012956	29.4	−0.043692	60.0
11	IM-p	−550.979035	29.0	0.012947	30.8	−0.043362	62.3
12	IM-ma	−550.980228	26.4	0.012964	28.3	−0.043719	58.8
13	IM-mb	−550.980036	25.9	0.012915	27.6	−0.042903	60.4
14	TS-s	−550.983996	16.0	0.011267	13.4	−0.039440	59.6
15	TS-oa	−550.971018	50.1	0.012006	49.4	−0.039470	93.7
16	TS-ob	−550.972080	47.3	0.012230	47.2	−0.040736	87.5
17	TS-p	−550.970512	51.4	0.012288	51.5	−0.041043	90.8
18	TS-ma	−550.971596	48.6	0.012213	48.5	−0.040877	88.5
19	TS-mb	−550.970875	50.4	0.012197	50.2	−0.040604	90.9

[a] Denotes that the data is the sum of the species and HNO_3 molecule

[b] CR denotes the complex of reactants

basis sets. The vibrational frequency analyses were performed at the same level to identify the minimum or the transition state with no or solely an imaginary normal mode vibration. The intrinsic reaction coordinates (IRCs) [31] were calculated to confirm the connection of the transition state and the respective minima with a step-size of 0.02 amu$^{1/2}$bohr. In order to exam the reactions more reliably, the energies of all the species as well as the minimum energy paths (MEPs) were further refined with the accurate model chemistry method G3(MP2) [32, 33] at the B3LYP/6-311G(d,p) geometries, namely G3(MP2)//B3LYP/6-311G(d,p). Non-dynamic electronic correlations for all the species were examined with the complete active space self-consistent field (CASSCF) calculations [34–39] at CASSCF/6-311G(d,p) level with the active space (7,7) (seven active electrons distribute in seven active orbitals) for radicals and (6,6) for closed shell species. The dominant configuration coefficients of all the species are larger than 0.93 which indicates that the multi-reference-state feature can approximately be eliminated. Thermochemistry data were developed with the standard statistical thermodynamics in which the electron excitation energies (vertical) were calculated with the time dependent TD-B3LYP/6-311G(d,p) method and were truncated at 1.860 eV [40]. All electronic structure calculations were performed using the Gaussian-09 program [41]. The rate constants were evaluated in the temperature range of 200–2000 K by using the canonical variational transition-state theory (CVT) [42–45] and that incorporated with the small-curvature-tunneling (SCT) [46, 47] corrections proposed by Truhlar and co-workers combined in the POLYRATE 8.2 program [48], in which the necessary information should be supplied including the geometries and energies of the reactants, products, transition states, and those of a number of the selected points around the TS in the MEP as well as the energy gradients and the Hessian matrix for each of the points. For the reactions that do not have an energy barrier, the rate constants were only calculated with the CVT method by the VKLab program [49], where the SCT effect was neglected [50]. The over-all reaction rate (within 300–2000 K) was explored with the COMSOL software [51] in which a batch reactor was chosen.

Results and discussion

The structure as well as the symmetry and the electronic state for each of the reactants (Rs), intermediates (IMs), and the transition states (TSs) optimized with B3LYP/6-311G(d,p) are shown in Fig. 1, in which the numbering of the 19 species will be used in the further discussions. The G3(MP2) energies (internal energy at 0 K), enthalpy, and the Gibbs free energy corrections ($H_{corr.}$ and $G_{corr.}$ at 298.15 K without zero point energy, ZPE) and their relative (with respect to the sum of the reactants) values are listed in Table 1. The energy profiles in the potential energy surface are illustrated in Fig. 2 that involves the internal energies at 0 K and the Gibbs free energies at 298.15 K.

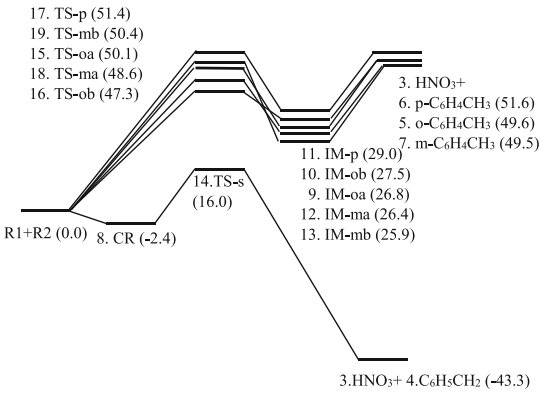

(a) relative internal energies at 0 K

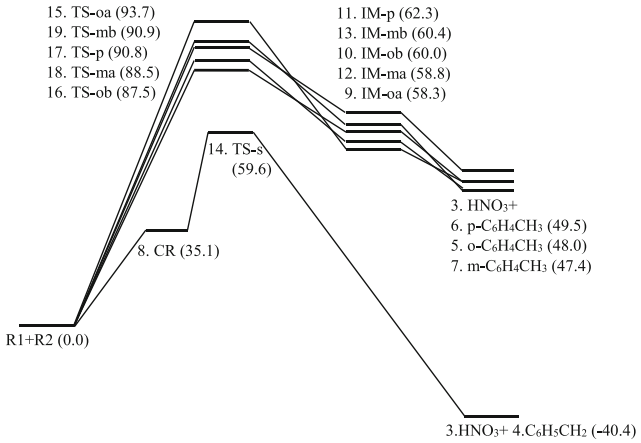

(b) relative Gibbs free energies at 298.15 K

Fig. 2 Energy profile for the hydrogen abstractions obtained with the G3(MP2)//B3LYP/6-311G(d,p) theoretical method. The data shown in the *parentheses* is the relative energy with respect to that of the sum of the reactants

Hydrogen abstraction

For the reaction of toluene with NO_3, a hydrogen atom can be abstracted from the side chain (methyl group) or from the benzene ring. It is shown in Fig. 2a that the lowest energy path is for the side chain H-abstraction reaction. At the entrance, a pre-reactive complex (CR, numbered 8, in ^{2}A' state) is formed with a weak van der Waals interaction. The internal energy is 2.4 kJ mol^{-1} lower than that of the sum of the reactants (R1+R2). It should be helpful for a detailed analysis of the electronic structure of 8.CR. For this purpose, we performed a complete active space self-consistent field CASSCF calculation and obtained a dominant state ^{2}A" that corresponds to an orbital alteration of the HOMO-3 and the LUMO of a beta

electron. However, this state was finally confirmed less stable either at B3LYP/6-311G(d,p) or at MP2/6-311G(d,p) level of theory.

Subsequently, 8.CR may decompose into the products ($3.HNO_3$+$4.C_6H_5CH_2$) via 14.TS-s with a small energy barrier of 18.4 kJ mol^{-1}. In 14.TS-s, the new forming O-H bond is about 1.416 Å, which is about 0.445 Å longer than that in the nitric acid molecule HNO_3. The breaking C-H bond is 1.220 Å, about 0.124 Å longer than the equilibrium distance in toluene. The change of the C-H distance is thus much smaller than that of the O-H. This may predict that 14.TS-s is a reactant-like transition state or the reaction proceeds via an early barrier. The HNO_3 molecule is now a less active species but the benzyl radical, a C_{2v} perfect planar structure, has the spin density 0.7887 mainly localized on the dehydrogenated carbon atom in the -CH_2 group. Its further degradation reactions that have not been involved in the scope of the present work must be a complicated but very interesting topic for future investigations.

The data in Table 1 also show that the whole reaction is thermodynamically favorable with 43.3 kJ mol^{-1} lowering of the energy, or is exothermic with 45.8 kJ mol^{-1} lowering of the enthalpy and is spontaneous with 40.4 kJ mol^{-1} lowering of the Gibbs free energy at 298.15 K.

For the abstraction of an ortho, para, and meta hydrogen atom from the benzene ring, the pre-reactive complex was not found but five transition states 15.TS-oa, 16.TS-ob, 17.TS-p, 18.TS-ma, and 19.TS-mb were located as shown in Fig. 1. Among those, both 15.TS-oa and 16.TS-ob are for the H-abstraction on the ortho position but distinguished with the positions of the H-bonds. This is due to that, in the rotation of the O18-N bond, different hydrogen bonds O19-H9 and O19-H14 can be formed. The relative energies of 15.TS-oa and 16.TS-ob are 50.1 and 47.3 kJ mol^{-1} with respect to the reactants, which are so close to each other that both of the paths should be taken into account for the ortho hydrogen abstraction reaction rate evaluations. In the 15.TS-oa and 16.TS-ob structures, the breaking C4-H12 bonds are 0.226 and 0.237 Å longer than the equilibrium distances, and the forming H12a-O18 and H12b-O18 bonds are 0.247 and 0.242 Å longer than the O-H bond in HNO_3, respectively. These similar changes may not support an obvious early or later barrier. By performing the IRC calculations starting from the corresponding transition states, the van der Waals complexes 9.IM-oa and 10.IM-ob at the exit of the channels are found which have energies of 23.3 and 19.8 kJ mol^{-1} lower than their corresponding transition states. The C4-H12 bond

Table 2 Rate constants (CVT/SCT, in $cm^3 \cdot molecule^{-1} \cdot s^{-1}$) of the side-chain and the first step ring H-abstractions of toluene and NO_3 radical as a function of temperature within 200–2000 K

T	k_s [a]	k_2	k_3	k_4	k_5	k_6	k [b]	Γ [c] / %
200	9.31×10^{-18}	4.46×10^{-28}	9.93×10^{-27}	5.31×10^{-27}	1.47×10^{-26}	2.61×10^{-27}	9.31×10^{-18}	100.0
298	1.42×10^{-17}	8.25×10^{-24}	1.13×10^{-22}	8.52×10^{-23}	1.37×10^{-22}	3.92×10^{-23}	1.42×10^{-17}	100.0
300	1.44×10^{-17}	9.50×10^{-24}	1.29×10^{-22}	9.78×10^{-23}	1.57×10^{-22}	4.50×10^{-23}	1.44×10^{-17}	100.0
400	3.56×10^{-17}	2.02×10^{-21}	2.17×10^{-20}	1.98×10^{-20}	2.76×10^{-20}	9.08×10^{-21}	3.57×10^{-17}	99.8
500	1.02×10^{-16}	5.99×10^{-20}	5.74×10^{-19}	5.91×10^{-19}	7.56×10^{-19}	2.70×10^{-19}	1.04×10^{-16}	97.8
600	2.73×10^{-16}	6.44×10^{-19}	5.82×10^{-18}	6.52×10^{-18}	7.83×10^{-18}	2.95×10^{-18}	2.93×10^{-16}	92.0
700	6.38×10^{-16}	3.82×10^{-18}	3.34×10^{-17}	3.98×10^{-17}	4.56×10^{-17}	1.79×10^{-17}	7.57×10^{-16}	82.0
800	1.31×10^{-15}	1.55×10^{-17}	1.32×10^{-16}	1.66×10^{-16}	1.83×10^{-16}	7.44×10^{-17}	1.8×10^{-15}	69.6
900	2.44×10^{-15}	4.84×10^{-17}	4.08×10^{-16}	5.33×10^{-16}	5.69×10^{-16}	2.37×10^{-16}	3.95×10^{-15}	57.6
1000	4.19×10^{-15}	1.25×10^{-16}	1.05×10^{-15}	1.41×10^{-15}	1.47×10^{-15}	6.26×10^{-16}	8.12×10^{-15}	47.2
1100	6.81×10^{-15}	2.81×10^{-16}	2.38×10^{-15}	3.25×10^{-15}	3.30×10^{-15}	1.43×10^{-15}	1.57×10^{-14}	39.0
1200	1.05×10^{-14}	5.67×10^{-16}	4.77×10^{-15}	6.69×10^{-15}	6.67×10^{-15}	2.93×10^{-15}	2.86×10^{-14}	32.7
1300	1.54×10^{-14}	1.05×10^{-15}	8.81×10^{-15}	1.26×10^{-14}	1.24×10^{-14}	5.51×10^{-15}	4.92×10^{-14}	27.6
1400	2.18×10^{-14}	1.81×10^{-15}	1.52×10^{-14}	2.21×10^{-14}	2.14×10^{-14}	9.64×10^{-15}	8.06×10^{-14}	23.7
1500	3.00×10^{-14}	2.96×10^{-15}	2.48×10^{-14}	3.67×10^{-14}	3.50×10^{-14}	1.59×10^{-14}	1.26×10^{-13}	20.6
1600	4.01×10^{-14}	4.61×10^{-15}	3.85×10^{-14}	5.79×10^{-14}	5.46×10^{-14}	2.51×10^{-14}	1.91×10^{-13}	18.2
1700	5.26×10^{-14}	6.91×10^{-15}	5.76×10^{-14}	8.76×10^{-14}	8.18×10^{-14}	3.79×10^{-14}	2.8×10^{-13}	16.2
1800	6.75×10^{-14}	1.00×10^{-14}	8.33×10^{-14}	1.28×10^{-13}	1.19×10^{-13}	5.52×10^{-14}	3.98×10^{-13}	14.6
1900	8.53×10^{-14}	1.41×10^{-14}	1.17×10^{-13}	1.82×10^{-13}	1.67×10^{-13}	7.82×10^{-14}	5.51×10^{-13}	13.2
2000	1.06×10^{-13}	1.93×10^{-14}	1.60×10^{-13}	2.52×10^{-13}	2.29×10^{-13}	1.08×10^{-13}	7.47×10^{-13}	12.1

[a] Side chain H-abstraction rate constant defined in Eq. (2)

[b] Sum of the rate constants k_s and k_{2-6}

[c] Ratio of side chain H-abstraction defined in Eq. (4)

distances are 2.012 and 2.011 Å in 9.IM-oa and 10.IM-ob showing a considerable interaction of the H-bond. By decomposing 9.IM-oa and 10.IM-ob, the same products, a less active 3.HNO_3 and the 5.o-$C_6H_4CH_3$ radical, can be formed with increasing energies of 22.8 and 22.1 kJ mol^{-1} but with decreasing Gibbs free energies of 10.3 and 12.0 kJ mol^{-1}.

For the para position, only one transition state 17.TS-p, and the associated product complex 11.IM-p, was found due to the symmetry of toluene. The energy barrier is 51.4 kJ mol^{-1} and is also the highest barrier found in this work and, is also a value that is well known for a reaction to proceed at an adequate rate around room temperatures. The complex 11.IM-p is 29.0 kJ mol^{-1} higher in energy with respect to the reactants, and it may further decompose into 3.HNO_3 and 6.p-$C_6H_4CH_3$ with an energy absorption of 22.6 kJ mol^{-1} but with a Gibbs energy releasing of 12.8 kJ mol^{-1}.

For the meta position, this work also found two transition states 18.TS-ma and 19.TS-mb as well as their produced complexes 12.IM-ma and 13.IM-mb are distinguished by the position of the H-bonds. The relative energies of these transition states are 48.6 and 50.4 kJ mol^{-1} higher than the reactants. Again, the small difference of the barriers represents that both of the paths should be taken into account in the further investigations.

It should be noted that, although the five complexes (numbered 9.IM-oa to 13.IM-mb) are stable in energy, their Gibbs free energies at 298.15 K are higher than those of the sum of the dissociated HNO_3 and a radical (5.o-$C_6H_4CH_3$ or 6.p-$C_6H_4CH_3$ or 7.m-$C_6H_4CH_3$) due to the increase of the entropy as shown in Fig. 2b. The relative (with respect to the reactants) Gibbs free energy for the dissociations are 48.0, 49.5, and 47.4 kJ mol^{-1}, corresponding to the equilibrium constant in the magnitude of ppb, a value that is difficult to be observed experimentally. Compared with the process of side chain H-abstraction, the ring H-abstractions are less favorable since the energy barriers are at least 31.3 kJ mol^{-1} higher. Additionally, the products 3.HNO_3+4.$C_6H_5CH_2$ from the side chain abstraction are much more stable than either of the 9.IM-oa to 13.IM-mb complexes or their dissociated species. The negative relative Gibbs free energy (−40.4 kJ mol^{-1}) corresponds to an equilibrium constant of 1.2×10^7 for the side chain H-abstraction reaction. This, therefore, confirmed thermodynamically that the side chain H-abstraction is dominant at least for 298.15 K.

Rate constants

The rate constants for all of the reaction steps were calculated with the CVT and CVT/SCT methods as mentioned in the previous section in which the G3(MP2)//B3LYP/6-311G(d,p) energies were employed both for the stationary points and for the minimum energy path (MEP). The temperature range is examined within 200–2000 K.

For the side chain H-abstraction, since a pre-reactive complex (CR) is produced with a very small energy decrease of 2.4 kJ mol^{-1}, a two-step mechanism that involves a fast equilibrium between the reactants and the pre-reactive complex is assumed as:

$$C_6H_5CH_3 + NO_3 \underset{}{\overset{K_{eq.}}{\longleftrightarrow}} CR \underset{k_{-1}}{\overset{k_1}{\longleftrightarrow}} HNO_3 + C_6H_5CH_2 \quad (1)$$

The forward rate constant for side chain hydrogen abstraction, k_s, becomes:

$$k_s = K_{eq}k_1 = \sigma\frac{Q_{CR}}{Q_{toluene}\cdot Q_{NO_3}}\exp\left(\frac{E_R - E_{CR}}{RT}\right)k_1 \quad (2)$$

where $K_{eq.}$ is the equilibrium constant between the reactants and the complex (CR), Q denotes the partition function of the related species, E_R and E_{CR} are the total energies (internal energy at 0 K) of reactants and CR, σ is the reaction symmetry number and R is the molar gaseous constant 8.314472 J·$mol^{-1}\cdot K^{-1}$.

Table 3 Decomposition rate constants (CVT, in s^{-1}) of the IMs formed in the first step ring H-abstractions

T	k_2'	k_3'	k_4'	k_5'	k_6'
200	2.01×10^{10}	5.25×10^{9}	2.02×10^{10}	6.58×10^{11}	7.94×10^{9}
298	1.52×10^{11}	6.90×10^{9}	1.34×10^{11}	4.60×10^{11}	9.69×10^{9}
300	1.57×10^{11}	6.91×10^{9}	1.38×10^{11}	4.57×10^{11}	9.69×10^{9}
400	4.60×10^{11}	6.73×10^{9}	3.54×10^{11}	3.38×10^{11}	8.74×10^{9}
500	8.97×10^{11}	5.95×10^{9}	4.88×10^{11}	2.62×10^{11}	7.22×10^{9}
600	1.41×10^{12}	5.08×10^{9}	6.07×10^{11}	2.11×10^{11}	5.79×10^{9}
700	1.92×10^{12}	4.29×10^{9}	7.13×10^{11}	1.74×10^{11}	4.61×10^{9}
800	1.80×10^{12}	3.61×10^{9}	8.10×10^{11}	1.47×10^{11}	3.68×10^{9}
900	1.71×10^{12}	3.04×10^{9}	8.98×10^{11}	1.27×10^{11}	2.95×10^{9}
1000	1.65×10^{12}	2.57×10^{9}	9.81×10^{11}	1.11×10^{11}	2.39×10^{9}
1100	1.61×10^{12}	2.18×10^{9}	1.06×10^{12}	9.79×10^{10}	1.95×10^{9}
1200	1.58×10^{12}	1.87×10^{9}	1.13×10^{12}	8.73×10^{10}	1.61×10^{9}
1300	1.56×10^{12}	1.61×10^{9}	1.20×10^{12}	7.85×10^{10}	1.33×10^{9}
1400	1.55×10^{12}	1.39×10^{9}	1.26×10^{12}	7.11×10^{10}	1.11×10^{9}
1500	1.54×10^{12}	1.21×10^{9}	1.32×10^{12}	6.47×10^{10}	9.38×10^{8}
1600	1.53×10^{12}	1.06×10^{9}	1.38×10^{12}	5.93×10^{10}	7.96×10^{8}
1700	1.53×10^{12}	9.27×10^{8}	1.44×10^{12}	5.45×10^{10}	6.80×10^{8}
1800	1.52×10^{12}	8.19×10^{8}	1.49×10^{12}	5.03×10^{10}	5.84×10^{8}
1900	1.52×10^{12}	7.26×10^{8}	1.54×10^{12}	4.66×10^{10}	5.05×10^{8}
2000	1.52×10^{12}	6.46×10^{8}	1.59×10^{12}	4.33×10^{10}	4.39×10^{8}

For the ring H-abstractions, the processes should be described as:

$$C_6H_5CH_3 + NO_3 \left\{ \begin{array}{l} \xrightarrow[k_{-2}]{k_2} \text{IM-oa} \xrightarrow[k_{-2'}]{k_{2'}} \\ \xrightarrow[k_{-3}]{k_3} \text{IM-ob} \xrightarrow[k_{-3'}]{k_{3'}} \end{array} \right\} \text{o-}C_6H_4CH_3 + HNO_3$$
$$\xrightarrow[k_{-4}]{k_4} \text{IM-p} \xrightarrow[k_{-4'}]{k_{4'}} \text{p-}C_6H_4CH_3 + HNO_3 \quad (3)$$
$$\left. \begin{array}{l} \xrightarrow[k_{-5}]{k_5} \text{IM-ma} \xrightarrow[k_{-5'}]{k_{5'}} \\ \xrightarrow[k_{-6}]{k_6} \text{IM-mb} \xrightarrow[k_{-6'}]{k_{6'}} \end{array} \right\} \text{m-}C_6H_4CH_3 + HNO_3$$

The numerical results of all the rate constants as a function of temperature within 200–2000 K are listed in Tables 2 and 3 and are shown in Fig. 3. In order to facilitate the reaction branching, a side chain rate branching ratio Γ that assumes all the reactions are irreversible can be defined as:

$$\Gamma = \frac{k_s}{k} = \frac{k_s}{\sum k_i} \quad (4)$$

with i=s, 2, 3, …, 6 as shown in Eqs. (2) and (3). The results are also listed in Table 2.

Figure 3 shows that all the CVT and CVT/SCT rate constants increase with increasing temperature or have positive temperature dependence. The CVT and CVT/SCT rate constants are basically close to each other within the temperature range 200–2000 K with the exception of the side chain H-abstraction that is quite different in its order of magnitude in

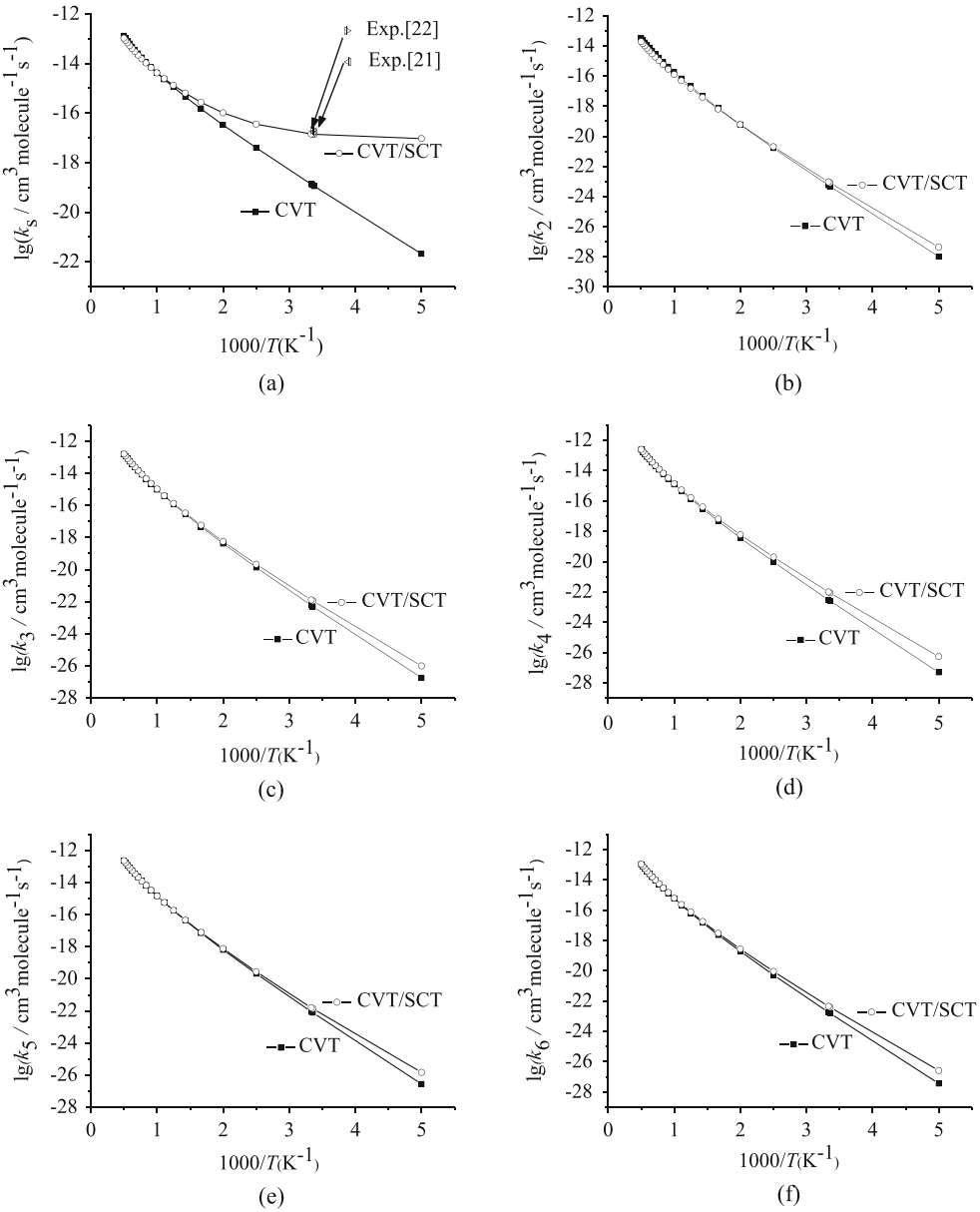

Fig. 3 Plots of the H-abstraction rate constants versus 1000/T (K^{-1}) in the temperature range 200–2000 K. (**a**) is for the side-chain, (**b**) for ortho-a, (**c**) for ortho-b, (**d**) for para, (**e**) for meta-a, and (f) for the meta-b H-abstractions. Experimental values shown in panel (**a**) are from refs. [21, 22]

the low temperature range. Interestingly, the CVT/SCT values of k_s shown in Fig. 3a are very close to the available experimental points [21, 22].

In investigating the magnitude of the rate constants in Table 2, it is found that the reaction proceeds exclusively through side chain H-abstraction below room temperature or mainly through this path within 400–700 K. This result is consistent with the experimental findings that the NO_3 radical only abstracts the side chain hydrogen at low temperatures [21, 24]. Our values, 1.40×10^{-17} $cm^3\cdot molecule^{-1}\cdot s^{-1}$ at 296 K and 1.42×10^{-17} $cm^3\cdot molecule^{-1}\cdot s^{-1}$ at 298 K are also in very good agreement with the observed side chain H-abstraction rate constants $(1.8\pm1.0)\times10^{-17}$ $cm^3\cdot molecule^{-1}\cdot s^{-1}$ [21] and $(2.0\pm1.1)\times10^{-17}$ $cm^3\cdot molecule^{-1}\cdot s^{-1}$ [22] at the correspondence temperatures. The theoretical value from ref. [28] is slightly larger in digit by 6.96 with the same order.

Although the experimental reaction rates for higher temperatures are unavailable, our results show that the ratio Γ for the side chain H-abstractions above 700 K decreases with increasing temperatures. For example, the ratio is 82.0 % at 700 K and is below 50 % (47.2 % at 1000 K, a smaller value from two more reaction channels (15.TS-oa and 19.TS-mb) on the ring compared with the larger theoretical value 68% of ref. [28]).

The relative values of the rate constants for the ring H-abstractions, as expected, are consistent with the magnitudes of the relative Gibbs free energies of the transition states that govern the rate constants in the CVT principles [42–48]. For example, k_2 for the rate constant via TS-oa is always smaller than the others due to TS-oa has the highest activation Gibbs free energy shown in Fig. 2b. Consequently, k_3 to k_6 have only slightly different values also due to the similar activation Gibbs free energies.

For the next decomposition of the ring H-abstractions intermediates, it is found in Table 3 that the rate constants k_2' to k_6' have very large values due to very small activation energies (Fig. 2a). This reason also leads to the very small change of the rate constants with increasing temperature according to the Arrhenius expression. It is interesting to find that the values for the decompositions of IM-ob (k_3') and IM-mb (k_6') are about 2–3 orders smaller than the others although the activation energies (22.1 to 23.6 kJ mol^{-1}) are similar. This may mainly be from the differences of the entropy increases and of the positions of the variational transition state in the potential energy surfaces.

It should be helpful to have an analytical expression of the rate constants for the convenience of further reference. All the rate constants for both of the forward and the reverse reactions have been fitted into three-parameter Arrhenius expressions:

$$k = A \times T^n \times \exp\left(-\frac{E}{T}\right) \quad (5)$$

The results within 200–2000 K are listed in Table 4.

It is found that the correlation coefficients of the fit are larger than 0.94 and most of them are larger than 0.99. The smaller values (about 0.95) are found for k_1, k_{-1} and k_s in the side chain H-abstraction. This shows that the three-parameter expressions are in very good quality for further applications. However, the parameter E for either k_s or k_1 is a negative value indicating that the rate constant for the decomposition of 8.CR as well as the over-all forward reaction of the side chain H-abstraction has non-Arrhenius characteristics. This might be from the larger tunneling effect at lower temperatures as shown in Fig. 3a. For the other elementary reactions having a transition state, the maximum error for the activation energies between the calculated in the fitted expressions and those shown in Table 1 (or Fig. 2a) is 10.2 kJ mol^{-1}. For the

Table 4 Fitted parameters A (in $cm^3\cdot molecule^{-1}\cdot s^{-1}$ if not specified), n and E for Eq.(4), and the fitting correlation coefficient R obtained within 200–2000 K for all the reactions in Eqs.(1) and (3)

Forward	A	n	E	R	Reverse	A	n	E	R
k_s	1.73×10^{-33}	5.98	−840.7	0.95594					
k_1	25.6 s^{-1}	3.26	−153.0	0.94966	k_{-1}	3.18×10^{-33}	5.97	4630.3	0.95573
k_2	2.85×10^{-25}	3.88	5150.9	0.99948	k_{-2}	3.13×10^{-4} s^{-1}	1.93	2212.5	0.99957
k_3	2.85×10^{-25}	3.88	4793.2	0.99925	k_{-3}	2.63×10^{7} s^{-1}	1.20	1747.6	0.99868
k_4	2.36×10^{-25}	3.98	4984.6	0.99927	k_{-4}	3.66×10^{7} s^{-1}	1.27	1765.4	0.99879
k_5	1.34×10^{-25}	4.02	4734.2	0.99807	k_{-5}	1.64×10^{7} s^{-1}	1.31	1889.6	0.99742
k_6	1.22×10^{-25}	3.95	4972.0	0.99908	k_{-6}	2.90×10^{7} s^{-1}	1.24	2081.2	0.99855
k_2'	8.11×10^{17} s^{-1}	−1.63	1805.7	0.96419	k_{-2}'	1.28×10^{-15}	1.26	−1184.5	0.99048
k_3'	1.58×10^{17} s^{-1}	−2.48	826.0	0.99811	k_{-3}'	1.71×10^{-16}	0.43	−1982.6	0.99924
k_4'	4.03×10^{13} s^{-1}	−0.37	1102.5	0.99055	k_{-4}'	2.36×10^{-20}	2.55	−1726.6	0.97776
k_5'	2.63×10^{15} s^{-1}	−1.44	134.1	0.99999	k_{-5}'	1.08×10^{-18}	1.48	−1168.7	0.99984
k_6'	5.33×10^{18} s^{-1}	−2.99	909.6	0.99806	k_{-6}'	1.83×10^{-15}	−0.07	−2118.5	0.99903

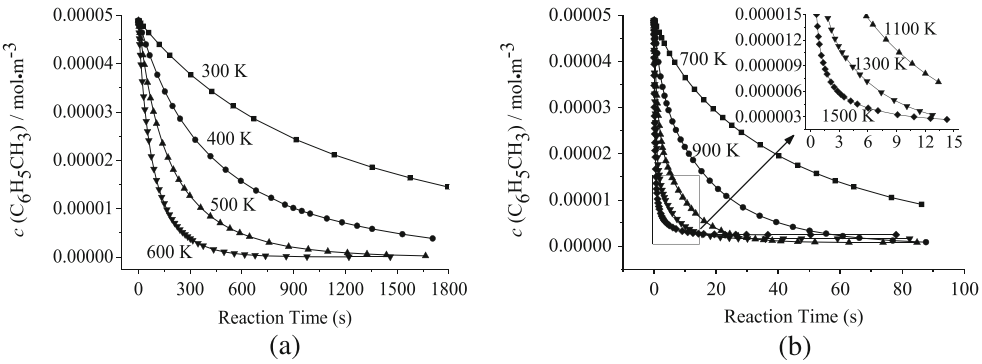

Fig. 4 Concentration of the reactant toluene versus the reaction time for 300–1500 K calculated with COMSOL [51], (**a**) for 300–600 K, (**b**) for 700–1500 K

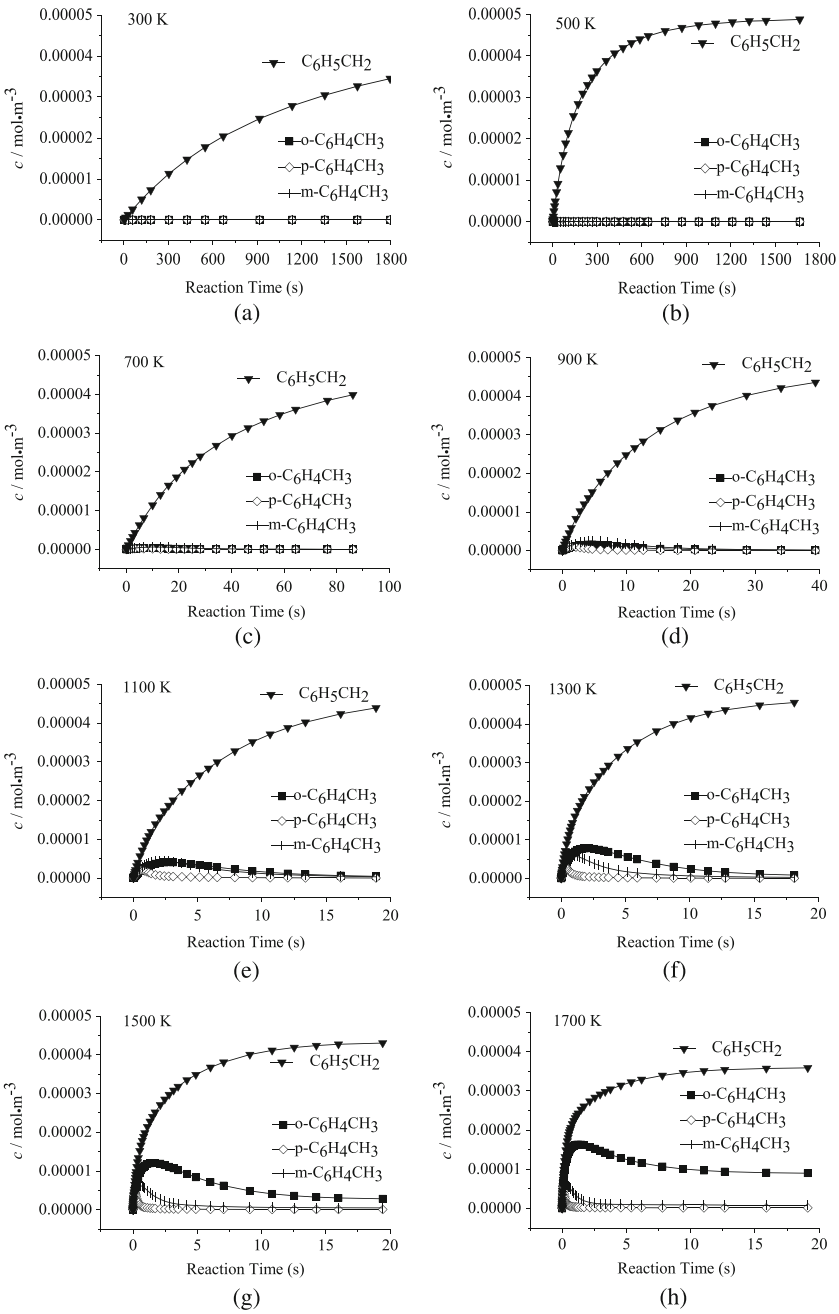

Fig. 5 Concentrations of the different products ($C_6H_5CH_2$, o-$C_6H_4CH_3$, p-$C_6H_4CH_3$, and m-$C_6H_4CH_3$) versus reaction time at 300–1700 K. (**a**) for 300 K, (**b**) for 500 K, (**c**) for 700 K, (**d**) for 900 K, (**e**) for 1100 K, (**f**) for 1300 K, (**g**) for 1500 K and (**h**) for 1700 K

elementary reactions without transition state, the activation energies are also comparable with the energy differences between the products and the intermediates. The results for the ring H-abstractions and dissociation reactions imply that the rate constant expressions are well Arrhenius characterized in the cases where the tunneling effect is small.

Reaction rate

In order to explore the over-all reaction rate, the concentration change of a reactant as a function of time needs to be developed. In the case of a complicated reaction, one needs to solve the coupled differential rate equations. Occasionally, an analytical expression can be obtained with, for example, the steady state approximation. However, the present work encountered that the concentrations of some intermediates were unable to be eliminated. Instead, numerical method can be employed and we simulated the reaction rate of NO_3 and toluene in a batch reactor with the COMSOL [51] package. The temperature range of 300–1500 K is examined for detailed reference especially for the significance of the ring H-abstractions. All the reactions are considered reversible and the initial concentrations of toluene and NO_3 radical are 4.9×10^{-5} and 8.3×10^{-5} mol/m^3, respectively. These values are the equivalent concentrations of the experiments of ref. [22]. The results for the over-all, i.e., all the reactions in both Eqs. (1) and (3), consumption of toluene are plotted in Fig. 4, where 4(a) is for temperatures of 300–600 K and 4(b) is for 700–1500 K.

Although a radical attacking reaction, possessing very low energy barrier, is generally a fast process, the reaction may also be slow if the concentration of a reactant is small. It is shown in Fig. 4a that the reactions are significant at room temperature with most of the reactant toluene to be consumed in about 30 minutes. The reaction rate increases, as expected, with increasing temperatures. It should be noted that the near-equilibrium concentration of toluene may have a larger value for a sufficient time at higher temperatures. For example, Fig. 4b shows that this occurs at about 15 s for 1500 K compared with that for 1300 K. This predicts that the over-all reaction is exothermic. For the reactions below 700 K, it is shown that the side chain H-abstraction is dominant which is consistent with the results obtained previously, e.g., the ratio Γ in Table 2, and the experiments [21, 24]. It should also be noted that the side chain H-abstraction is nearly irreversible since the concentration of toluene will approach a very low value (close to zero) for an extent of time below 700 K. For 700 K at 100 s, for example, the concentrations have a very small deviation of less than 0.17 % if the reaction is considered irreversible. This result is in good agreement of the much higher energy barrier in the reverse process shown in Fig. 2a.

The over-all reactions may have more complicated properties in the ring H-abstractions since three different products could be produced via five different parallel channels shown in Eq.(3). The concentrations of the products $C_6H_5CH_2$, o-$C_6H_4CH_3$, p-$C_6H_4CH_3$ and m-$C_6H_4CH_3$ as a function of reaction time for different temperatures of 300–1700 K are plotted in Fig. 5. It is shown that the concentration for the product of methyl H-abstraction $C_6H_5CH_2$ is always larger than others. The concentrations for those of the ring H-abstractions increase with temperature but they are not significant for temperatures below 700 K. For temperatures above 800 K (which has not been shown in Fig. 5 but 700 and 900 K can be referred), it is expectable to have the ring H-abstraction products observed. However, their concentrations have a maximum at a very short reaction time. The existence of the maximum concentration implies that the ring H-abstraction reactions are obviously reversible. Within the ring products, the concentration of the meta H-abstraction m-$C_6H_4CH_3$ is larger than the others for 900 K or 1100 K. However, that of the o-$C_6H_4CH_3$ becomes larger above 1300 K.

Therefore, the reactions within the system can be, qualitatively, regarded as the typical reaction below 700 K is the side chain H-abstraction and those above 800 K are the side chain and the ring H-abstraction challenging.

The logarithm overall reaction rates, donated by the consumption rates of toluene, versus the reciprocal temperatures are presented in Fig. 6. The nonlinearity relationship also shows that the over-all reaction follows a complex procedure. However, the apparent activation energy $E_{app.}$ of the reaction can be roughly estimated if the curve is divided into two parts, the side chain H-abstraction part below 700 K and the challenging reactions above 800 K. The fitted reaction rate r is $\ln r=-10.951-1862.9/T$ for 300–700 K and is $\ln r=-2.8811-7981.3/T$ for 800–2000 K with the correlation coefficients 0.9716 and 0.9934, respectively. This corresponds to the apparent activation energies $E_{app.}$ of 15.5 and 66.4 kJ mol^{-1}, and the values are comparable with the activation energies shown previously in Fig. 2a.

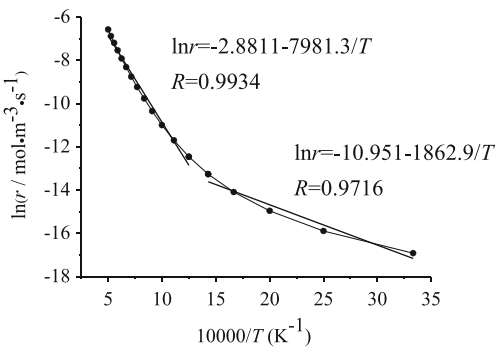

Fig. 6 Plots and fits of the overall reaction rate (denoted by the concentration decreasing rate of toluene for its initial concentration 4.9×10^{-5} mol/m^3) versus 10,000/T (K^{-1}) within 300–2000 K

Conclusions

The hydrogen abstraction reactions of toluene by NO_3 radical are studied theoretically by means of accurate ab initio and reaction kinetics methods. Both the side chain and the ring H-abstractions are examined and the properties of the reactions are explored in detail. It is found that the side chain H-abstraction has a larger tunneling effect and shows a non-Arrhenius characteristic. In contrast, the ring H-abstractions have smaller tunneling effect and follow the Arrhenius behavior well. The theoretical rate constant for the side chain H-abstraction at room temperature is in very good agreement with the available experiments. The over all reaction possesses a complicated reaction mechanism in which the side chain H-abstraction is dominant below 700 K and is nearly irreversible, while the ring H-abstractions are competitive above 800 K with observable products. The ring H-abstractions are also found typically reversible. The approximate apparent activation energies E_{app} are 15.5 and 66.4 kJ mol^{-1} at 300–700 K and 800–2000 K, respectively.

Acknowledgments Part of the calculations were performed in the High Performance Computation Center of the Northwestern Polytechnical University. This work was supported by the Nature Science Foundation of Shaanxi Province (2014JQ2074, 2014JQ6231) and the Foundation of Northwestern Polytechnical University (JCY20130144)

References

1. Seinfield JH, Pandis SN (1997) Atmospheric chemistry and physics: from air pollution to climate change. Wiley, New York
2. Dearth MA, Glerczak CA, Slegl WO (1992) Environ Sci Technol 26:1573–1581
3. Tanaka T, Samukawa T (1996) Chemosphere 33:131–145
4. Etzkorn T, Klotz B, Sørensen S, Partroescu IV, Barnes I, Becker KH, Platt U (1999) Atmos Environ 33:525–540
5. Odum JR, Jungkamp TPW, Griffin RJ, Flagan RC, Seinfeld JH (1997) Science 276:96–99
6. Schwartz J, Dockery DW, Neas LM (1996) J Air Waste Manag Assoc 46:927–939
7. Derwent RG, Jenkin ME, Saunders SM (1996) Atmos Environ 30: 181–199
8. Calvert JG, Atkinson R, Becker KH, Kamens RM, Seinfeld JH, Wallington TJ, Yarwood G (2002) The mechanisms of atmospheric oxidation of aromatic hydrocarbons. Oxford University Press, Oxford
9. Atkinson R, Arey J (2003) Chem Rev 103:4605–4638
10. Atkinson R (1989) J Phy Chem Ref Data, Monograph 1:1–246
11. Smith DF, Mciver CD, Kleindienst TE (1998) J Atmos Chem 30: 209–228
12. Perry RA, Atkinson R, Pitts JN Jr (1977) J Phys Chem 81:296–304
13. Tully FP, Ravishankara AR, Thomson RL, Nicovich JM, Shah RC, Kreutter NM, Wine PH (1981) J Phys Chem 85:2262–2269
14. Schuler RH, Albarranb G (2002) Radiat Phys Chem 64:189–195
15. Anderson PN, Hites RA (1996) Environ Sci Technol 30:301–306
16. Baltaretu CO, Lichtman EI, Hadler AB, Elrod MJ (2009) J Phys Chem A 113:221–230
17. Koch R, Knispel R, Elend M, Siese M, Zetzsch C (2007) Atmos Chem Phys 7:2057–2071
18. Seta T, Nakajima M, Miyoshi A (2006) J Phys Chem A 110:5081–5090
19. Uc VH, Alvarez-Idaboy JR, Galano A, García-Cruz I, Vivier-Bunge A (2006) J Phys Chem A 110:10155–10162
20. Carter WPL, Winer AM, Pitts JN Jr (1981) Environ Sci Technol 15: 829–831
21. Atkinson R, Carter WPL, Plum CN, Winer AM, Pitts JN Jr (1984) Int J Chem Kinet 16:887–898
22. Atkinson R, Plum CN, Carter WPL, Winer AM, Pitts JN Jr (1984) J Phys Chem 88:1210–1215
23. Atkinson R, Aschmann SM (1988) Int J Chem Kinet 20:513–539
24. Atkinson R, Arey J (2007) Polycycl Aromat Comp 27:15–40
25. Fenter FF, Nozière B, Caralp F, Lesclaux R (1994) Int J Chem Kinet 26:171–189
26. Silva G, Chen CC, Bozzelli JW (2007) J Phys Chem A 111:8663–8676
27. Murakami Y, Oguchi T, Hashimoto K, Nosaka Y (2007) J Phys Chem A 111:13200–13208
28. Huang MQ, Liao YM, Wang ZY, Hao LQ, Zhang WJ (2014) Comput Theor Chem 1037: 63–69
29. Becke AD (1993) J Chem Phys 98:5648–5652
30. Lee C, Yang W, Parr RG (1988) Phys Rev B 37:785–789
31. Gonzalez C, Schlegel HB (1990) J Phys Chem 94:5523–5527
32. Curtiss LA, Redfern PC, Raghavachari K, Rassolov V, Pople J (1999) J Chem Phys 110:4703–4709
33. Baboul AG, Curtiss LA, Redfern PC, Raghavachari K (1999) J Chem Phys 110:7650–7657
34. Hegarty D, Robb MA (1979) Mol Phys 38:1795–1812
35. Eade RHE, Robb MA (1981) Chem Phys Lett 83:362–368
36. Schlegel HB, Robb MA (1982) Chem Phys Lett 93:43–46
37. Bernardi F, Bottini A, McDougall JJW, Robb MA, Schlegel HB (1984) Faraday Symp Chem Soc 19:137–147
38. Yamamoto N, Vreven T, Robb MA, Frisch MJ, Schlegel HB (1996) Chem Phys Lett 250:373–378
39. Frisch MJ, Ragazos IN, Robb MA, Schlegel HB (1992) Chem Phys Lett 189:524–528
40. Deng JL, Su KH, Zeng Y, Wang X, Zeng QF, Cheng LF, Xu YD, Zhang LT (2008) Physica A 387:5440–5456
41. Frisch MJ, Trucks GW, Schlegel HB, Scuseria GE, Robb MA, Cheeseman JR, Scalmani G, Barone V, Mennucci B, Petersson GA, Nakatsuji H, Caricato M, Li X, Hratchian HP, Izmaylov AF, Bloino J, Zheng G, Sonnenberg JL, Hada M, Ehara M, Toyota K, Fukuda R, Hasegawa J, Ishida M, Nakajima T, Honda Y, Kitao O, Nakai H, Vreven T, Montgomery JA Jr, Peralta JE, Ogliaro F, Bearpark M, Heyd JJ, Brothers E, Kudin KN, Staroverov VN, Kobayashi R, Normand J, Raghavachari K, Rendell A, Burant JC, Iyengar SS, Tomasi J, Cossi M, Rega N, Millam JM, Klene M, Knox JE, Cross JB, Bakken V, Adamo C, Jaramillo J, Gomperts R, Stratmann RE, Yazyev O, Austin AJ, Cammi R, Pomelli C, Ochterski JW, Martin RL, Morokuma K, Zakrzewski VG, Voth GA, Salvador P, Dannenberg JJ, Dapprich S, Daniels AD, Farkas O, Foresman JB, Ortiz JV, Cioslowsk J, Fox DJ (2009) Gaussian 09, revision A.02. Gaussian Inc, Wallingford
42. Garrett BC, Truhlar DG (1979) J Chem Phys 70:1593–1598
43. Baldridge KK, Gordor MS, Steckler R, Truhlar DG (1989) J Phys Chem 93:5107–5119
44. Gonzalez-Lafont A, Truong TN, Truhlar DG (1991) J Chem Phys 95:8875–8894
45. Garrett BC, Truhlar DG (1979) J Phys Chem 83:1052–1079
46. Liu YP, Lynch GC, Truong TN, Lu D, Truhlar DG, Garrett BC (1993) J Am Chem Soc 115:2408–2415
47. Lu DH, Truong TN, Melissas VS, Lynch GC, Liu YP, Grarrett BC, Steckler R, Issacson AD, Rai SN, Hancock GC, Lauderdale JG, Joseph T, Truhlar DG (1992) Comput Phys Commun 71:235–262

48. Chuang YY, Corchado JC, Fast PL, Villa J, Hu WP, Liu YP, Lynch GC, Jackels CF, Nguyen K, Gu MZ, Rossi I, Coitino E, Clayton S, Melissas VS, Lynch BJ, Steckler R, Garret BC, Isaacson AD, Truhlar DG (1999) POLYRATE, version8.2. University of Minnesota, Minneapolis
49. Zhang SW, Truong TN (2001) VKLab, version 1.0. University of Utah, Salt Lake City
50. Li QS, Zhang Y, Zhang SW (2005) J Mol Model 11:41–47
51. Comsol Multiphysics, Version 3.4, Comsol, Inc.: Los Angeles, CA, available at http://www.comsol.com